July 1997

Resonance feature in Al^- photodetachment below the $Al(3s^2 4s\ ^2S)$ threshold

B.J. Davies
University of Virginia, Charlottesville

C.W. Ingram
University of Virginia, Charlottesville

D.J. Larson
University of Virginia, Charlottesville

Chien-Nan Liu
University of Nebraska - Lincoln

Anthony F. Starace
University of Nebraska-Lincoln, astarace1@unl.edu

Resonance feature in Al^- photodetachment below the $Al(3s^2 4s\ ^2S)$ threshold

B. J. Davies, C. W. Ingram, and D. J. Larson
Department of Physics, University of Virginia, Charlottesville, Virginia 22901

Chien-Nan Liu and Anthony F. Starace
Department of Physics and Astronomy, The University of Nebraska, Lincoln, Nebraska 68588-0111

(Received 26 November 1996)

Photodetachment of $Al^-(3s^2 3p^2\ ^3P)$ near the threshold of the first excited state of neutral aluminum has been studied both experimentally and theoretically. A 19-keV mass-resolved Al^- beam was intersected by a frequency-doubled neodymium-doped yttrium aluminum garnet pumped dye-laser beam, and the fast atoms created by detachment processes were detected. Measurements just below the threshold of the first excited state, $Al(3s^2 4s\ ^2S)$, find a large resonance peak in the detachment signal. An eigenchannel R-matrix calculation generates a resonance structure that is qualitatively similar to the data and identifies the large resonance peak as resulting from a doubly excited negative-ion state having predominantly $(3s^2 4s4p\ ^3P^o)$ character. Density plots of the resonance state are presented to demonstrate its structure. Near the $Al(3s^2 3p\ ^2P)$ threshold, theory agrees also with recent relative measurements of D. Calabrese *et al.* [Phys. Rev. A **54**, 2797 (1996)]. [S1050-2947(97)08606-X]

PACS number(s): 32.80.Gc, 31.25.Jf

I. INTRODUCTION

Observations of the properties of doubly excited autoionizing states in multielectron systems can provide detailed information on electron-electron correlations and stringent experimental checks for multielectron theory. One of the most interesting and demanding processes available for these studies is the photoexcitation of doubly excited negative ions in negative-ion photodetachment. Photoexcitation provides precise control of the excitation energy and final states (via the dipole selection rules), while negative ions allow the opportunity to observe electron-electron correlation which is not masked by the Rydberg levels typical of neutral atom or positive ion spectra.

Several studies of doubly excited negative ion states have been undertaken by observing resonance structure in the total detachment cross section. These resonances result from the interference between the continuum detachment channel and the detachment through the autoionizing state, as described by Fano in 1961 [1]. To date, the most thorough investigation of these resonances is for the hydrogen negative ion. These studies include measurements of the cross section for photodetachment from H^- near the thresholds for excitation to the first several excited states of H [2–4], revealing a series of resonances approaching several of the excited-state thresholds. The resonances observed [4] below the higher excitation thresholds have been interpreted theoretically [5–10] as reflecting propensity rules for populating particular channels of so-called ''+''-type doubly excited states.[1]

Comparable measurements have been performed for the alkali metals at their first atomic excited state [13–17], and for Li^- at higher excited states [18]. Pan, Starace, and Greene [19,20] carried out eigenchannel R-matrix calculations, and Lindroth [21] has carried out complex coordinate rotation calculations which are in excellent agreement with the experimental results for Li^- [18]. Pan, Starace, and Greene [19,20] showed that the propensity rules found for H^- photodetachment also apply to Li^-, although the non-Coulomb core in the latter case gives rise to additional kinds of doubly excited states which are not seen in H^-. The theoretical calculations for Li^- exploit the fact that it shares with H^- an s^2 ground-state configuration, and hence treat only two active electrons.

Photoexcitation resonance measurements on the potentially more complicated p-subshell negative ions have only begun recently, and few negative ion systems have been studied. Amusia *et al.* [22] presented theoretical calculations for Si^- which predict strong correlation effects for intershell transitions. These were confirmed experimentally by Balling *et al.* [23]. Intershell effects in B^- have also recently been studied both experimentally [24] and theoretically [25]. The Al^- negative ion studied here may also have strong correlation effects near intershell transition thresholds. However, these lie at higher energies than are considered in this work. Very recently the relative photodetachment cross section for Al^- near the detachment threshold has been measured [26].

The experimental and theoretical results presented here concern a doubly excited state in the photodetachment of Al^- near the threshold for the first excited atomic state. A simplified level diagram of the aluminum ion-atom system is shown in Fig. 1. The electron affinity of aluminum has recently been measured to be $3556.4(+5.3/-3.9)\,cm^{-1}$ [26]. This low electron affinity of the atom combined with the low energies of the first several excited states allows single-photon detachment in the vicinity of the first four excited states using readily available dye-laser technology. The configuration of the ground state of the negative ion is best

[1]The ''+'' and ''−'' doubly excited-state notation was introduced in Ref. [11] to denote linear combinations of independent particle states for He having either enhanced (''+'') or diminished (''−'') probability amplitude in the vicinity of the He ground state; these states corresponded to the experimentally observed [12] strong and weak series of doubly excited states in He photoionization spectra.

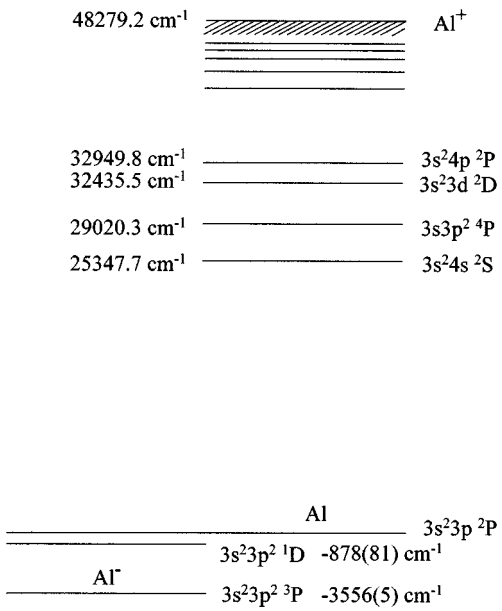

FIG. 1. Level diagram of the aluminum negative ion and atom. All energies shown are between the lowest of the fine-structure states and the Al $3s^2 3p(^2P_{1/2})$ ground state.

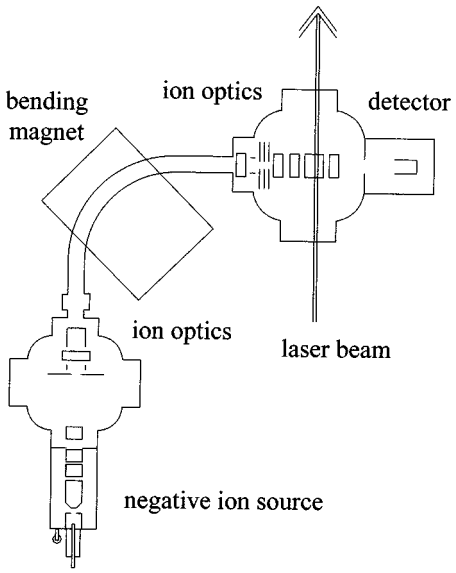

FIG. 2. Schematic diagram of the negative ion beam apparatus.

described as $3s^2 3p^2(^3P)$. The best values available for the ground-state fine-structure splittings are 26(3) cm^{-1} for the $^3P_0 \rightarrow {}^3P_1$ transition and 76(7) cm^{-1} for the $^3P_0 \rightarrow {}^3P_2$ transition [27]. In addition to the ^3P negative-ion state, there is a ^1D state which is bound by only 878(81) cm^{-1} [28].

When photodetaching in the energy region near the excited atomic states, the detachment channel directly to the ground-state atom is already open, of course, and can provide a substantial detachment signal. The Al $3s^2 3p(^2P)$ ground state has a fine-structure splitting of 112 cm^{-1} [29]. The experiments reported here explored the relative cross section near the threshold for the first excited state, which is located at an energy of 25347.7 cm^{-1} with respect to the ground state, and has an approximate configuration of $3s^2 4s(^2S)$.

Eigenchannel R-matrix calculations for the photodetachment of Al^- $3s^2 3p^2(^3P^e)$ from threshold to the first excited state of Al are presented. These calculations treat only the outer two electrons as active, and ignore the effects of intershell transitions involving the $3s$ subshell, since these occur at higher energies than are explored experimentally in this work. The theoretical results find a resonance that is in qualitative agreement with the present experiments. Furthermore, the theoretical results characterize the nature of the observed resonance. Comparison is also made to the recent measurements near threshold [26].

II. EXPERIMENT

The experiment described here was performed using a negative-ion beam intersected by a frequency-doubled dye-laser beam. The negative ions were produced by a cesium sputter source and mass separated by a 90° bending magnet. In the interaction region, the ion beam carried 100–500 pA, and was about 1 mm in diameter. The laser beam was generated by doubling the light from a neodymium-doped yttrium aluminum garnet (Nd:YAG)-pumped dye-laser operating in the 690-nm range. The laser had a repetition rate of 20 Hz, which set the time scale for the data acquisition. After exposure to the laser light, the number of neutral atoms produced was recorded using a time-resolved channeltron-based detection system. Although the ion-beam apparatus has undergone substantial modification, many of its components were described in detail in Ref. [30], so only those aspects which have been modified will be discussed here. Figure 2 is a schematic diagram of the ion beam apparatus.

The source is a SNICS II (source of negative ions by cesium sputtering), whose operation has been thoroughly described in Ref. [30]. In this source Cs^+ ions strike a negatively biased sputter target. Negative ions formed by this collision process are electrostatically extracted from the source and focused into a beam. Since the ions are formed on a surface of fixed potential, the resulting beam is essentially monoenergetic. Because Al^- is less prolific than the ions used in our previous work with the SNICS II [30–32], the source parameters were substantially modified in order to maximize current output. For this work, the sputtering energy is about 7 keV, while the extraction potential is 12 kV, thus producing an ion beam with a kinetic energy of 19 keV. Although a sputter target of 99% pure aluminum metal is used, the current of atomic and molecular negative ions from sputter target impurities and background gas (at 10^{-7} torr) dwarfs the Al^- current. It is therefore necessary to separate different mass components of the ion beam.

Mass analysis is accomplished using a sector magnet with a 90° bend. Since the ion beam is of a single-charge state, and has a small energy spread (on the order of 0.1%), the velocity-dependent magnetic force provides mass separation of the different components present in the ion beam. The magnet has a mass-energy product (which specifies the largest energy for which a given mass can pass through the magnet) of 5 MeV amu. In addition to simply providing mass separation, the magnet is designed to provide stigmatic focusing from the magnet's entrance aperture to its exit aperture. Because the quality of the magnetic focusing depends

strongly on the divergence of the input beam, a significant aberration occurs for the configuration used in this experiment owing to the input beam divergence of approximately 40 mrad. Although the mass separation at low masses (near 27 amu for Al^-) was unimpaired by the aberration, the transmission rate through the magnet was rather low, resulting in barely acceptable losses in the Al^- current. The mass resolution in the configuration used has been measured to be about one in 200.

After passing through the exit aperture of the magnet, the ion beam is electrostatically focused and steered into the laser-beam–ion-beam interaction region about 20 cm away. This 20 cm of ion optics includes some corrective steering plates as well as two sets of vertical deflection plates which shift the ion beam axis upwards by 1.5 cm just before the interaction region. This vertical displacement reduces the collisionally induced background signal by preventing the neutral atoms created by collisional stripping before the deflection plates from passing into the interaction region and reaching the detectors. Following the displacement, the ion beam enters the interaction region through a 1-mm aperture, and is intersected at 90° by the laser beam. Immediately after the interaction region, another set of vertical deflection plates is used to separate the charge states of the beam. Those negative ions which survive the interaction with the light are angled upward at about 14° into a Faraday cup, allowing continuous computer monitoring of the ion current. The undeflected neutral atoms are detected with a channeltron. Careful screening of the detector from the line of sight of the laser-beam path, combined with a mesh at the entrance of the channeltron held at -3 kV, eliminates signal due to stray electrons.

In these experiments, the detector signal is amplified and then integrated. The integration gate is approximately 20-ns wide. The integrated signal is transferred to a personal computer (PC) after every laser pulse along with the no-laser integrator background level so that any slow drift in the detection electronics can be removed. The PC also allows continuous monitoring of the relative laser energy and ion current, and this information is recorded after every laser shot to allow data normalization during later analysis.

The laser system consists of a pulsed dye laser (PDL), pumped by the second harmonic of a Nd:YAG laser. The PDL generates 5 ns pulses of red light, which are then frequency doubled using a potassium dihydrogen phosphate (KDP) crystal to produce 346-nm light. Three ultraviolet mirrors are used to direct the 346-nm light into the vacuum system and through the interaction region. These mirrors also serve to remove the undoubled visible light from the laser beam by attrition, since each mirror reflects only a few percent of the visible light. With the KDP crystal mistuned so as to produce negligible amounts of 346-nm light, the remaining visible light produces no measurable photodetachment signal. The frequency of the visible dye-laser light is calibrated using a monochrometer which had previously been calibrated with the emission lines of a mercury lamp. This yields a calibration of the 346-nm light with an accuracy of better than 1 cm^{-1}. The laser beam's energy per pulse is measured by sampling the light leaving the vacuum chamber. The time-averaged laser power for the UV light was about 20 mW.

We note that the ionization potential (E_{IP}) of aluminum is only 48279.2 cm^{-1}, and the energy of the first excited state is thus more than half of E_{IP}. The frequency of the photodetaching light in these experiments is therefore sufficient to photoionize any of the excited atomic states. For the lower excited states, at least, such photoionization would be nonresonant, however, and is therefore both small and only slowly varying with photon energy. Its influence on the data near the excited state is ignored.

III. THEORY

The eigenchannel R-matrix method employed in this work for photodetachment of negative ions has been described in detail very recently elsewhere [20]. For this reason, here we discuss only some general features of the method. We then discuss some of the specific details of our treatment of Al^- photodetachment.

The eigenchannel R-matrix method [33–36] aims to determine variationally a set of normal logarithmic derivatives of a system's wave function which are constant across a reaction surface S enclosing a reaction volume V. For treatments of two-electron excitations, the reaction volume V is that part of six-dimensional configuration space for which both electrons lie within a sphere of radius r_0. The reaction surface S is the set of points for which $\max(r_1,r_2)=r_0$, where r_1 and r_2 are the electron distances from the nucleus. In practice, for each range of excitation energy, r_0 is chosen to be sufficiently large that the probability of both electrons being outside r_0 is negligible. The complicated many-electron interactions within V are treated by bound-state, configuration-interaction techniques using independent electron functions and LS coupling. Normally r_0 is also chosen large enough so that long-range interaction effects may be neglected. In this work, however, all long-range multipole interactions for $r>r_0$ were treated numerically by close-coupling procedures, as in Refs. [19] and [20]. This permits much smaller values of r_0 to be used than would otherwise be the case.

In the present calculation, since the ground-state term of Al^- is $^3P^e$, electric dipole selection rules in LS coupling imply that the following channels are open just above the first excited state:

$$\begin{aligned}\gamma+\mathrm{Al}^-(3s^2 3p^2\ {}^3P^e) &\rightarrow \mathrm{Al}\ \ 3s^2 3p(^2P)\epsilon s(^3P^o)\\ &\rightarrow \mathrm{Al}\ \ 3s^2 3p(^2P)\epsilon d(^3P^o,{}^3D^o)\\ &\rightarrow \mathrm{Al}^*\ \ 3s^2 4s(^2S)\epsilon p(^3P^o). \qquad (1)\end{aligned}$$

(Note that in the above expressions only the leading configurations are indicated; in our calculations all states have an LS-coupled, multiconfiguration representation.) Since the photon energy range in this experiment is below the threshold of the $3s\rightarrow 3p$ intershell transition, we represent Al^- by two $3p$ valence electrons moving in a model potential describing the Al^+ core. The model potential has the form

$$V(r)=-\frac{1}{r}[Z_c+(Z-Z_c)e^{-a_1 r}+a_2 r e^{-a_3 r}]$$

$$-\frac{\alpha_c}{2r^4}(1-e^{-(r/r_c)^3})^2. \quad (2)$$

In this equation, the nuclear charge is $Z=13$, the charge of the Al^+ core is $Z_c=1$, and the polarizability of the Al^+ ion is taken to be $\alpha_c=26.25$ a.u. [37]. The parameters a_1, a_2, a_3, and r_c in Eq. (2) are determined by fitting the energy levels predicted by the potential in Eq. (2) to experimental Al energy levels [29] and thus include implicitly effects of configuration mixing in the atom.

Inside an R-matrix sphere having $r_0=60$ a.u., 18 closed-type (i.e., zero at $r=r_0$) and two open-type (i.e., nonzero at $r=r_0$) one-electron radial wave functions are calculated for each of the orbital angular momenta $0\leqslant l\leqslant 3$. These constitute the basis in which we expand our two-electron states. We describe the initial state by 150 two-electron configurations formed from these one electron basis wave functions. We include 337 (392) closed-type, two-electron configurations in the R-matrix calculation for the $L=1$ (2) final state. Furthermore, for each channel in which one electron can escape from the reaction volume, we include two open-type orbitals for the outer electron in addition to the closed-type basis orbitals.

Finally, in addition to photodetachment partial cross sections we also calculate probability density distributions for the state responsible for the resonance feature in the partial cross section. As was done in Refs. [19] and [20], these probability density distributions are extracted from a separate calculation for discrete resonance states as follows: All basis functions were set to zero on the boundary of the interaction volume V. Thus only the discrete levels were calculated; one of them occurred at the energy of the resonance feature in the cross section. We have calculated this state's probability density distribution in three ways: in (r_1,r_2) coordinates, in (α,θ_{12}) hyperspherical coordinates [where $\alpha \equiv tan^{-1}(r_2/r_1)$], and in (μ,λ) prolate spheroidal coordinates [where $\mu\equiv(r_1-r_2)/r_{12}$ and $\lambda\equiv(r_1+r_2)/r_{12}$]. The latter two probability density distributions are calculated at the peak of the resonance's probability amplitude in the hyperspherical radius $R\equiv(r_1^2+r_2^2)^{1/2}$. For the probability density in (r_1,r_2), we integrated the probability density over all angles $(\hat{\mathbf{r}}_1,\hat{\mathbf{r}}_2)$.

IV. RESULTS

A. Experimental observations

Photodetachment data near the threshold for the $3s^24s(^2S)$ aluminum state are shown in Fig. 3. The neutral atom signal is proportional to the total photodetachment cross section from the ^3P ion state, except for the possible presence of a roughly constant baseline. This baseline, whose magnitude is difficult to determine, results from the nonresonant photodetachment of those aluminum ions initially in the ^1D state and from photodetachment or photodissociation of any 27-amu molecular ions which may be present in the beam. The location of the threshold, with respect to the lowest-lying fine structure level of the negative-ion ground state, is indicated by the marker from below at 28 927 cm^{-1}. The width of the marker indicates the uncertainty in the location of the threshold, which results almost entirely from the uncertainty in the electron affinity.

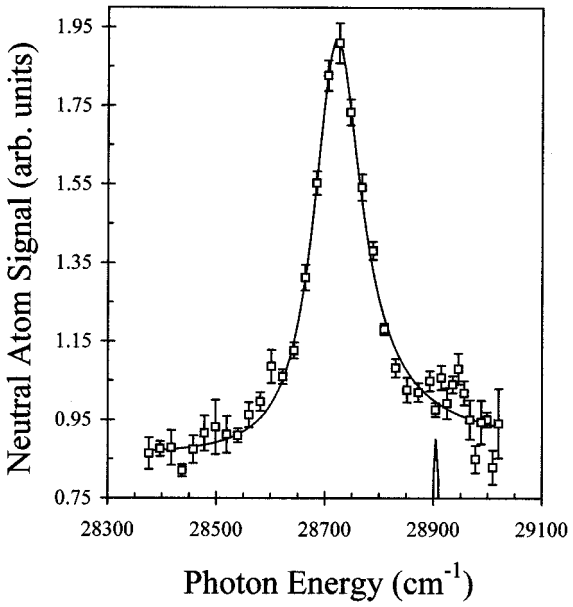

FIG. 3. Photodetachment data below the Al $3s^24s(^2S)$ threshold along with the result of a Beutler-Fano profile fit to the observed resonance. The best-fit parameters are $q=12.4$, $\Gamma=108$ cm^{-1}, and $E_{res}=28\,717$ cm^{-1} with a reduced χ^2 of 2.65. The marker indicates the energy of the atomic state with respect to the $3s^23p^2(^3P_0)$ negative ion state. The width of the marker indicates the uncertainty in the threshold position.

The large peak in the detachment signal, located about 200 cm^{-1} below the threshold, is strong evidence for the existence of a doubly excited, autodetaching Feshbach state associated with the $3s^24s$ parent atomic state. The doubly excited state is best described, according to our theoretical results, as a $3s^24s4p(^3P^o)$ state. The peak in the signal appears to be slightly asymmetric, rising more sharply on the low-energy side. In addition, the signal level away from the peak on the high-energy side is larger than that on the low-energy side. The presence of this asymmetry is consistent with the usual characteristics of Feshbach resonances. In addition to the large resonance, the data weakly suggest the presence of additional structure near the threshold. Additional data are needed to determine whether or not any such structure actually exists.

The structure observed can be reasonably well parameterized by a simple Beutler-Fano profile [1] plus a baseline, which can be written as

$$S=A\left[\frac{(q+\varepsilon)^2}{1+\varepsilon^2}\right]+B, \quad (3)$$

where S is the neutral atom signal, A is the value of the resonant component of the signal far away from the resonance, and B is the nonresonant background signal. Here q is the lineshape parameter and ε is a scaled energy parameter

$$\varepsilon = \frac{\hbar\omega - E_{\rm res}}{\Gamma/2}, \tag{4}$$

where $\hbar\omega$ is the photon energy, $E_{\rm res}$ is the location of the resonance, and Γ is the energy width of the resonance. The result of a Beutler-Fano profile fit to the data is shown in Fig. 3 along with the data. With a reduced χ^2 of 2.65, the best-fit parameters are found to be $q=12.4\pm2.7$, $\Gamma=108\pm6$ $\rm cm^{-1}$, and $E_{\rm res}=28717\pm3$ $\rm cm^{-1}$. The multiplier A is 6.8×10^{-3}, and the nonresonant background B is 8.6×10^{-1}. The large value for q is in marked contrast to hydrogen or the heavier alkali metals, where window resonances were observed [2–4,13–15], or for silicon, where the resonance fit gave a q value of about one-half [23]. Instead, the large value of q in this case gives the resonance a nearly symmetric profile. It is worth noting that the value of q obtained from the fit is sensitive to the inclusion of the data on the higher-energy side of the resonance (above 28 850 $\rm cm^{-1}$). If these data are removed from the fit, a reduced χ^2 of 1.60 is found, giving a resonance parameter $q=34$. Excluding the higher-energy data and fitting to the case of $q=\infty$ produces a reduced χ^2 of 1.64, only slightly worse than the previous case. Also, the sign of q is not well determined. Thus all we can confidently conclude is that the magnitude of q is very large. Furthermore, the very small value of A (which is proportional to the fractional part of the continuum with which the resonance interacts [38,39]) indicates that this resonance interacts with only a very small portion of the underlying continuum; rather, the resonance profile essentially sits atop the continuum.[2]

B. Theoretical predictions

An overview of the Al^- photodetachment cross section from threshold to the region of the experimentally observed resonance below 29 000 $\rm cm^{-1}$ is shown in Fig. 4. This figure shows dipole length results of our eigenchannel R-matrix calculation. One observes that near threshold the cross section is dominated by the $^3P^o$ partial cross section [cf. Eq. (1)].[3] The inset figure compares our dipole length and velocity results with the recent relative experimental measurements of Calabrese *et al.* [26]. Excellent agreement with these measurements is seen, except possibly for the highest-energy measured data point, which indicates a drop in cross section which we do not predict. Away from threshold the $^3D^o$ partial cross section [cf. Eq. (1)] becomes the dominant one. Our dipole velocity results for the total detachment cross section are within 15% of the dipole length results from threshold to 20 000 $\rm cm^{-1}$. Above that energy dipole length and velocity results differ by more than that, as shown in Fig. 5 for the region of the newly observed resonance. We have no explanation for the large difference in our dipole length and velocity results in the higher-energy region but note that differences of similar magnitude in negative-ion photodetachment calculations have been obtained by others [42].

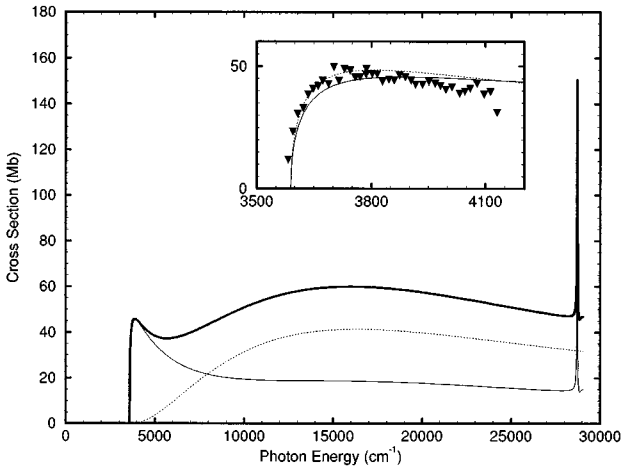

FIG. 4. Theoretically predicted photodetachment cross section for Al^- from threshold to just above the first excited Al threshold using an eigenchannel R-matrix approach and the dipole length approximation. Thick solid curve: total cross section. Dotted curve: $^3D^o$ partial cross section [cf. Eq. (1)]. Thin solid curve: $^3P^o$ partial cross section [cf. Eq. (1)]. The inset shows dipole length (solid curve) and velocity (dotted curve) theoretical results in comparison with the relative measurements of Calabrese *et al.* [26].

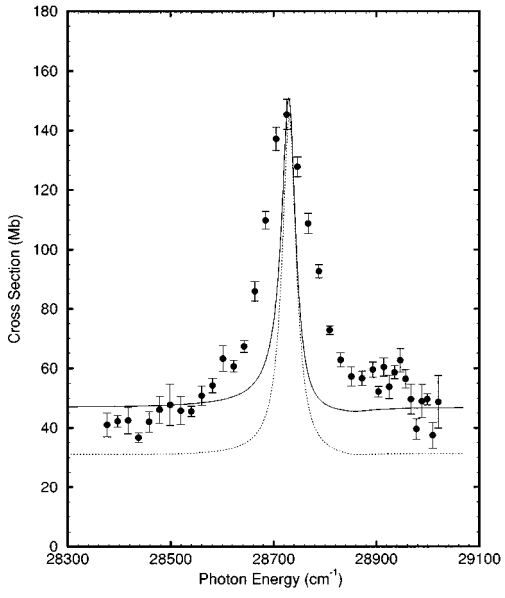

FIG. 5. Theoretically predicted total photodetachment cross section for Al^- in the photon energy region just below the first excited state threshold. Both dipole length (solid curve) and velocity (dashed curve) results are shown. Relative experimental data from Fig. 3 have been fit to the dipole length theoretical results using two parameters: the magnitude of the background cross section and the scaling factor to put the data on an absolute basis.

[2]Writing Eq. (3) in the form [38,39] $\sigma(E)=\sigma_c(E)\{\rho^2[(q+\epsilon)^2/(1+\epsilon^2)]+1-\rho^2\}$, where $\sigma_c(E)$ is the cross section outside the resonance region and ρ^2 is the ''maximal fractional depth of the depression of the continuous absorption spectrum'' [40], we find that $\rho^2=A/(A+B)\approx7.8\times10^{-3}$, thereby indicating that the observed resonance only interacts with about 0.78% of the continuum.

[3]This dominance stems from the Wigner threshold law [41] and the fact that the $^3P^o$ partial cross section has an $l=0$ photoelectron channel contribution whereas the $^3D^o$ partial cross section only has an $l=2$ photoelectron channel contribution.

The newly observed narrow resonance below 29 000 cm^{-1} dominates the total cross section, more than tripling its magnitude, as shown in Fig. 4. Furthermore, this resonance affects only the $^3P^o$ partial cross section and not the $^3D^o$ one. In Fig. 5 we present our dipole length and velocity eigenchannel R-matrix predictions for the total cross section over the photon energy region, 28 300 $cm^{-1} \leq \hbar\omega \leq 29\,100$ cm^{-1}. The experimentally measured relative results from Fig. 3 are compared with our theoretical predictions by normalizing the data to our results after subtracting a constant background. (Note that the magnitude of the background is not known experimentally; for the purposes of comparison with theory, the magnitude of the background and of the factor needed to put the relative data on an absolute scale were chosen to give the best overall agreement with our dipole length predictions.) One sees that theory and experiment are in quite close agreement on the position of the resonance. Also, theory and experiment both exhibit a roughly symmetric resonance (i.e., having a high value of $|q|$). There are, however, differences in the details of the line shape. Theory predicts a substantially narrower resonance than is observed experimentally. Theory also does not confirm the structure observed experimentally on the high energy side of the resonance in the vicinity of the $Al(3s^2 4s\ ^2S)$ threshold. (Indeed, our calculations predict no structure associated with the opening of the excited-state channel.) Finally, theory predicts a high *negative* value for the line shape parameter q, while experiment observes a high *positive* q value. It may be that the structure observed experimentally on the high-energy side of the resonance is affecting the sign of q in the experimental fitting. Also, it may be that intershell transitions from the $3s$ subshell (which we neglect) must be included to obtain the correct width of this resonance, although it is not clear that this should necessarily be so. We plan to investigate the effect of such intershell transitions, particularly at higher photon energies, in future theoretical studies.

We have also carried out additional calculations in order to characterize the newly observed resonance, as described in Sec. III above. Figure 6 shows probability densities for the discrete resonance state plotted in three different ways: in (r_1, r_2) coordinates [Fig. 6(a)]; in hyperspherical angle coordinates (α, θ_{12}) for $R \equiv (r_1^2 + r_2^2)^{1/2} = 15$ a.u. [Fig. 6(b)]; and in prolate spheroidal coordinates (μ, λ) for $R = 15$ a.u. [Fig. 6(c)]. As shown clearly in Fig. 6(b), this resonance has its maximum amplitude for $\alpha = \pi/4$ (or, $r_1 = r_2$) and $\theta_{12} = \pi$. It is thus a ''+'' -type state similar to those predicted to dominate the photodetachment spectrum of H^- [5–10]. As for labeling this resonance, we note that in our multiconfiguration representation for this state the largest configuration components are $4s4p(^3P^o)$ (probability $= 56\%$) and $4s5p(^3P^o)$ (probability $= 30\%$). Thus one may describe it approximately as the $4s4p(^3P^o)$ doubly excited state.

While the radial correlations of this state are best described by the ''+'' label, the angular correlations may be described approximately by the K and T quantum numbers of Herrick and Kellman [43] and Lin [44]. In terms of these quantum numbers, the $4s4p(^3P^o)$ resonance may be described by $(K = 3$ and $T = 0)^+$. In terms of the molecular classification scheme applied to H^- photodetachment [8,9], this state clearly has no nodes in θ_{12} and hence has vibrational quantum number $v = 0$. Hence, it may also be labeled as ${}_N\{v\}_n^+ = {}_4\{0\}_4^+$, where N and n are the principal quantum numbers of the inner and outer doubly excited electrons. These classification schemes are useful for describing similar probability distributions of doubly excited states [e.g., compare our Fig. 6(b) results for this $4s4p(^3P^o)$ resonance with Fig. 13 of [44] for $1snp(^3P^o)$ probability distributions for the $e^- - H$ or $e^- - He^+$ systems].

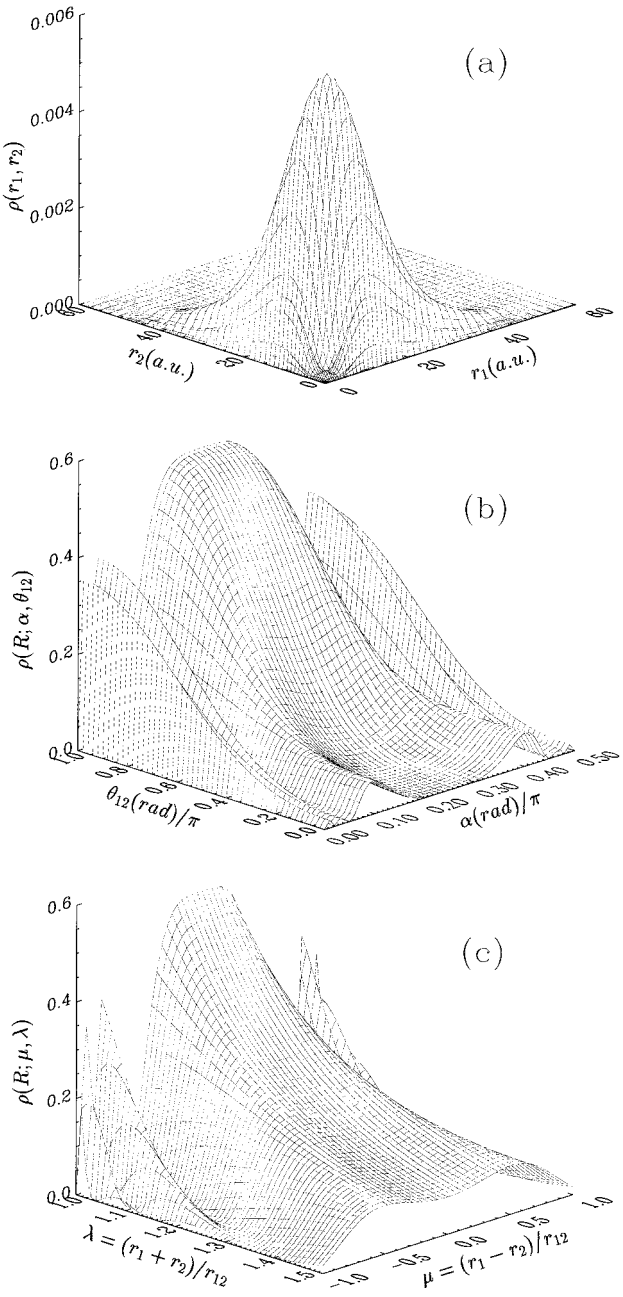

FIG. 6. Theoretically calculated probability density distribution for the predicted doubly excited $4s4p(^3P^o)$ resonance state plotted in three ways: (a) Plotted vs (r_1, r_2) with dependence on angular variables integrated over. (b) For $R \equiv (r_1^2 + r_2^2)^{1/2} = 15$ a.u., plotted vs (α, θ_{12}), where $\alpha \equiv \tan^{-1}(r_2/r_1)$. (c) For $R = 15$ a.u., plotted vs prolate spheroidal coordinates (μ, λ) (cf. Sec. III).

Note also that for H^- photodetachment it was found theoretically that only $v = 0$ doubly excited states were significantly populated. A similar propensity rule was found to ap-

ply to Li^- photodetachment [19,20], although the nonhydrogenic core in that case leads to the population of a few other states as well (which, however, have lesser prominence than the $v=0$ resonances). The present results are the first prediction for such a $v=0$ propensity rule in a triplet doubly-excited-state photodetachment spectrum.

V. CONCLUSIONS

The relative photodetachment cross section of Al^- in the vicinity of the Al $3s^2 4s(^2S)$ threshold has been measured using an Al^--ion beam intersected by a frequency doubled dye-laser beam. A large, narrow, nearly symmetric resonance signal was observed below this threshold. Eigenchannel R-matrix calculations for photodetachment of Al^- (using an approximation in which only the outer-two electrons are active) give predictions for the cross section from the Al $3s^2 3p(^2P)$ threshold up to the Al $3s^2 4s(^2S)$ threshold. Near the former threshold the theoretical predictions are in excellent agreement with recent relative measurements of Calabrese *et al.* [26]. Just below the Al $3s^2 4s(^2S)$ threshold, theory predicts a sharp, nearly symmetric resonance at the same energy observed experimentally. The theoretical line shape for this resonance agrees qualitatively with experiment, but is significantly narrower, possibly due to neglect of intershell transitions involving the $3s$ subshell. Also, theory does not confirm the experimentally observed structure in the high-energy wing of the resonance about the Al $3s^2 4s(^2S)$ threshold. The theoretical calculations indicate that the observed resonance is predominantly $4s4p(^3P^o)$, having a correlation structure indicated approximately by $(K,T)^A=(3,0)^+$ [43,44]. In other words, the observed state is a doubly excited electronic configuration having a large antinode when the two electrons lie on either side of the nucleus ($\theta_{12}=\pi$); furthermore, the two-electron wave function has no nodes as a function of θ_{12}.

ACKNOWLEDGMENTS

The authors thank J. E. Thoma for his experimental assistance, and C. H. Greene, C. D. Lin, F. Robicheaux, and H. Sadeghpour for valuable discussions. They also thank D. Calabrese and J. W. Farley for providing their data prior to publication. The work of B.J.D., C.W.I., and D.J.L. was supported in part by the National Science Foundation under Grant No. PHY-9313771. The work of C.N.L. and A.F.S. was supported in part by the U.S. Department of Energy, Division of Chemical Sciences, Office of Basic Energy Sciences under Grant No. DE-FG03-96ER14646.

[1] U. Fano, Phys. Rev. **124**, 1866 (1961).
[2] M. E. Hamm, R. W. Hamm, J. Donahue, P. A. M. Gram, J. C. Pratt, M. A. Yates, R. D. Bolton, D. A. Clark, H. C. Bryant, C. A. Frost, and W. W. Smith, Phys. Rev. Lett. **43**, 1715 (1979).
[3] H. C. Bryant, B. D. Dieterle, J. Donahue, H. Sharifian, H. Tootoonchi, D. M. Wolfe, P. A. M. Gram, and M. A. Yates-Williams, Phys. Rev. Lett. **38**, 228 (1977).
[4] P. G. Harris, H. C. Bryant, A. H. Mohagheghi, R. A. Reeder, H. Sharifian, C. Y. Tang, H. Tootoonchi, J. B. Donahue, C. R. Quick, D. C. Rislove, W. W. Smith, and J. E. Stewart, Phys. Rev. Lett. **65**, 309 (1990).
[5] H. R. Sadeghpour and C. H. Greene, Phys. Rev. Lett. **65**, 313 (1990).
[6] J. M. Rost and J. S. Briggs, J. Phys. B **23**, L339 (1990).
[7] J. M. Rost, J. S. Briggs, and J. M. Feagin, Phys. Rev. Lett. **66**, 1642 (1991).
[8] H. R. Sadeghpour, Phys. Rev. A **43**, 5821 (1991).
[9] H. R. Sadeghpour, C. H. Greene, and M. Cavagnero, Phys. Rev. A **45**, 1587 (1992).
[10] H. R. Sadeghpour and M. Cavagnero, J. Phys. B **26**, L271 (1993).
[11] J. W. Cooper, U. Fano, and F. Pratts, Phys. Rev. Lett. **10**, 518 (1963).
[12] R. P. Madden and K. Codling, Phys. Rev. Lett. **10**, 516 (1963).
[13] T. A. Patterson, H. Hotop, A. Kasadan, D. W. Norcross, and W. C. Lineberger, Phys. Rev. Lett. **32**, 189 (1974).
[14] J. Slater, F. H. Read, S. E. Novick, and W. C. Lineberger, Phys. Rev. A **17**, 201 (1978).
[15] P. Frey, F. Breyer, and H. Hotop, J. Phys. B **11**, L589 (1978).
[16] Y. K. Bae and J. R. Peterson, Phys. Rev. A **32**, 1917 (1985).
[17] J. Dellwo, Y. Liu, D. J. Pegg, and G. D. Alton, Phys. Rev. A **45**, 1544 (1992).
[18] U. Berzinsh, G. Haeffler, D. Hanstorp, A. Klinkmuller, E. Lindroth, U. Ljungblad, and D. J. Pegg, Phys. Rev. Lett. **74**, 4795 (1995).
[19] C. Pan, A. F. Starace, and C. H. Greene, J. Phys. B **27**, L137 (1994).
[20] C. Pan, A. F. Starace, and C. H. Greene, Phys. Rev. A **53**, 840 (1996).
[21] E. Lindroth, Phys. Rev. A **52**, 2737 (1995).
[22] M. Ya. Amusia, G. F. Gribakin, V. K. Ivanov, and L. V. Chernysheva, J. Phys. B **23**, 385 (1990).
[23] P. Balling, P. Kristensen, H. Stapelfeldt, T. Andersen, and H. K. Haugen, J. Phys. B **26**, 3531 (1993).
[24] P. Kristensen, H. H. Andersen, P. Balling, L. D. Steele, and T. Andersen, Phys. Rev. A **52**, 2847 (1995).
[25] C. A. Ramsbottom and K. L. Bell, J. Phys. B **28**, 4501 (1995).
[26] D. Calabrese, A. M. Covington, J. S. Thompson, R. W. Marawar, and J. W. Farley, Phys. Rev. A **54**, 2797 (1996).
[27] H. Hotop and W. C. Lineberger, J. Phys. Chem. Ref. Data **4**, 539 (1975).
[28] C. S. Feigerle, R. R. Corderman, and W. C. Lineberger, J. Chem. Phys. **74**, 1513 (1981).
[29] W. C. Martin and R. Zalubas, J. Phys. Chem. Ref. Data **8**, 817 (1979).
[30] N. D. Gibson, B. J. Davies, and D. J. Larson, Phys. Rev. A **47**, 1946 (1993).
[31] N. D. Gibson, B. J. Davies, and D. J. Larson, Phys. Rev. A **48**, 310 (1993).
[32] N. D. Gibson, B. J. Davies, and D. J. Larson, J. Chem. Phys. **98**, 5104 (1993).
[33] U. Fano and C. M. Lee, Phys. Rev. Lett. **31**, 1573 (1973).
[34] P. F. O'Mahony and C. H. Greene, Phys. Rev. A **31**, 250 (1985).

[35] C. H. Greene in *Fundamental Processes of Atomic Dynamics*, edited by J. S. Briggs, H. Kleinpoppen, and H. O. Lutz (Plenum, New York, 1988), pp. 105–127.
[36] C. H. Greene and L. Kim, Phys. Rev. A **36**, 2706 (1987).
[37] R. Szmytkowski and A. M. Alhasan, Phys. Scr. **52**, 309 (1995).
[38] U. Fano and J. W. Cooper, Phys. Rev. **137**, A1364 (1965); cf. Eqs. (1.1) and (2.12).
[39] U. Fano and J. W. Cooper, Rev. Mod. Phys. **40**, 441 (1968); cf. Sec. 8.1 and especially Eq. (8.5).
[40] Cf. Ref. [39], p. 494.
[41] See, e.g., U. Fano and A.R.P. Rau, *Atomic Collisions and Spectra* (Academic, New York, 1986), pp. 76 and 77.
[42] G. Miecznik and C. H. Greene, Phys. Rev. A **53**, 3247 (1996).
[43] D. R. Herrick and M. E. Kellman, Phys. Rev. A **21**, 418 (1980).
[44] C. D. Lin, Phys. Rev. A **29**, 1019 (1984).